doi.org/10.36721/PJPS.2026.39.4.REG.15414.1

Investigating the molecular mechanism of icariin in inhibiting liver cirrhosis carcinogenesis by regulating miR-145 based on the ROS-NLRP3 pathway

Yanfei Wang[1*], Xiangda Meng[2], Shimin Wang[3], Hongting Sui[4], Wenjuan Wang[5], Guohua Li[6], Liping Cong[1], Chao Wu[7], Ting Cao[8] and Jing Zhang[9]

[1]Department of Infectious Diseases, The First Affiliated Hospital of Qiqihar Medical University, Qiqihar, Heilongjiang, China
[2]Department of Otolaryngology, The First Affiliated Hospital of Qiqihar Medical University, Qiqihar, Heilongjiang, China
[3]Department of Traditional Chinese Medicine, Qiqihar Seventh College, Qiqihar, Heilongjiang, China
[4]Department of Respiratory and Critical Care Medicine, The First Affiliated Hospital of Qiqihar Medical University, Qiqihar, Heilongjiang, China
[5]Department of Statistics, The First Affiliated Hospital of Qiqihar Medical University, Qiqihar, Heilongjiang, China
[6]Department of Imaging, The First Affiliated Hospital of Qiqihar Medical University, Qiqihar, Heilongjiang, China
[7]School of Nursing, Qiqihar Medical University, Qiqihar, Heilongjiang, China
[8]College of Pathology, Qiqihar Medical University, Qiqihar, Heilongjiang, China
[9]Department of Clinical Medicine, Mudanjiang Medical University, Mudanjiang, Heilongjiang, China

Abstract: **Background**: Hepatocarcinogenesis arising from liver cirrhosis is a major contributor to hepatocellular carcinoma (HCC), but effective interventions remain limited **Objective**: This study aimed to elucidate the molecular mechanism by which icariin suppresses cirrhosis-to-cancer progression through the ROS/NLRP3/miR-145 axis. **Methods**: Fifty Sprague-Dawley rats were randomly assigned to five groups: control, model, low-dose icariin (ICA-L), high-dose icariin (ICA-H), and positive control. *In vitro*, SMMC-7721 and HepG2 cells were treated with TGF-β1 and various concentrations of icariin to assess their effects on hepatocellular carcinoma cell activity. **Results**: Compared with the model group, icariin significantly reduced the liver index, serum AFP levels, Ki-67 positivity, and hepatic ROS levels in rats, suppressed NLRP3 expression, upregulated miR-145, and effectively ameliorated liver fibrosis and dysplasia ($P<0.05$). In SMMC-7721 cells, icariin inhibited TGF-β1-induced proliferation, migration and invasion, promoted apoptosis and G0/G1 phase arrest, while concurrently increasing exosomal miR-145 levels ($P<0.05$). Further mechanism verification confirmed that miR-145 directly targets and inhibits NLRP3 expression. **Conclusion**: Icariin effectively inhibits cirrhosis-associated carcinogenesis by suppressing the ROS-NLRP3 pathway and upregulating miR-145, providing a theoretical basis for the prevention and treatment of cirrhosis and hepatocellular carcinoma.

Keywords: Carcinogenesis of cirrhosis; Hepatic stellate cells; Icariin; miR-145; ROS-NLRP3 pathway

Submitted on 21-10-2025 – Revised on 17-11-2025 – Accepted on 09-12-2025

INTRODUCTION

Hepatocellular carcinoma (HCC) is a leading causes of cancer-related deaths worldwide, and its development frequently occurs secondary to liver cirrhosis. Although the annual carcinogenesis rate in cirrhotic patients reaches 3-8%, effective clinical interventions to block this malignant transformation are currently lacking, resulting in a poor prognosis (Singal *et al*., 2023). In clinical practice, cirrhosis-associated hepatocellular carcinoma is primarily monitored using ultrasound imaging and serum alpha-fetoprotein (AFP) detection. The sensitivity and specificity of AFP are somewhat limited, particularly for AFP-negative hepatocellular carcinoma (ANHC), which is prone to being missed (Hwang *et al*., 2025). Therefore, identifying novel intervention targets has become a research priority. Icariin is a flavonoid extracted from the traditional Chinese medicine Epimedium. In a non-alcoholic fatty liver disease model, icariin promotes fatty acid oxidation by activating the AMPK pathway, inhibits lipid synthesis, and thereby reduces hepatocyte steatosis (Hai *et al*., 2023). Previous studies have shown that icariin exerts biological effects through miRNA regulation. (Rong *et al*., 2024). found significantly reduced miR-145 level in liver cancer ($P < 0.001$); Moreover, miR-145 level was correlate with tumors number ($P = 0.040$), vascular invasion ($P = 0.010$), Edmondson-Steiner grade ($P = 0.011$), BCLC stage ($P = 0.003$) (Shen *et al*., 2023), and survival (Lai *et al*., 2023). Given the regulatory potential of icariin on miRNAs and the tumor-suppressive role of miR-145 in liver cancer, we hypothesized that icariin may inhibit cirrhosis-associated carcinogenesis by upregulating miR-145 expression.

The ROS-NLRP3 inflammasome pathway is a key regulatory of the innate immune response. Reactive oxygen species (ROS) derived from mitochondrial dysfunction, cytochrome P450 system activation and metabolic activity of damaged hepatic stellate cells during liver cell damage serve as upstream triggers of this pathway (Carpi *et al*.,

**Corresponding author:* e-mail: woyongshan353539@126.com

2024). Studies have shown that modulation of the ROS-NLRP3 axis can alleviate hepatocyte apoptosis and necrosis (Wang *et al*., 2023). Zhai *et al.* (2022) further demonstrated that NOX4 promotes Kupffer cell inflammation via the ROS-NLRP3 pathway, exacerbating liver inflammatory injury. This indicates that abnormal activation of the ROS-NLRP3 pathway is a key driving of liver injury. Based on this background, we hypothesize that icariin inhibits hepatic ROS generation, suppresses NLRP3 inflammasome activation, upregulates tumor-suppressive miR-145, and thereby inhibits cirrhosis-associated carcinogenesis. To test this hypothesis, we systematically investigated the molecular mechanism by which icariin regulates miR-145 to inhibit hepatocellular carcinoma via the ROS-NLRP3 pathway, providing new theoretical insights for liver cancer treatment.

MATERIALS AND METHODS

Materials

Main reagents and antibodies

Icariin (Icariin, ICA, Jiangsu Yongjian Pharmaceutical, purity ≥98%); TGF-β1 (PeproTech); carbon tetrachloride (CCl4), olive oil and ethanol (Zhengzhou Hengtai Chemical Raw Materials LTD); Cell detection kits (BCA, CCK-8 and Annexin V-FITC/PI, all purchased from Fuyuan Biotechnology); ROS agonist 2-ME (MedChem Express), ROS inhibitor NAC (MedChemExpress); RIPA lysis buffer (Shanghai Xingqi Biotechnology); Transwell chambers (Beijing Mengzhuang Technology); miR-145 mimic, miR-145 inhibitor and negative control (Jima Gene); primary and secondary antibodies (Shanghai Boshenglong Biotechnology); Matrigel (Shanghai Mituo Biotechnology).

Instruments

Fluorescence microplate reader (for ROS detection): model SpectraMax iD5 (manufacturer: Molecular Devices), chemiluminescence imaging system (for Western blotting): model ChemiDoc MP (manufacturer: Bio-Rad), flow cytometer (for apoptosis detection): model BD Accuri C6 (manufacturer: BD Biosciences), light microscope (for histopathological observation): model Olympus BX53 (manufacturer: Olympus), microplate reader (for CCK-8 and ELISA): model Multiskan GO (manufacturer: Thermo Fisher Scientific).

Animal experiments

Experimental animals and grouping

Fifty Sprague-Dawley rats were randomly assigned to five groups (n=10 per group): control, model, low-dose icariin (50 mg/kg, ICA-L), high-dose icariin (100 mg/kg, ICA-H), and positive control (sorafenib, 10 mg/kg). Except for the control group, all rats received a single intraperitoneal injection of diethylnitrosamine (DEN) followed by intraperitoneal administration of 40% CCl_4 in olive oil (initial dose 5 mL/kg, followed by 3 mL/kg per administration, twice weekly) and 10% ethanol in drinking water for 12 weeks to establish a DEN/CCl_4-induced cirrhosis-carcinogenesis model (Uehara *et al*., 2021). The control group received equivalent volumes of saline and normal drinking water. After model induction, rats in each group received the corresponding treatments by gavage; control and model groups received saline.

Sample collection

After the last drug administration, the rats were fasted but allowed to drink water freely for 12 hours. After the fasting period, they were anesthetized and blood was collected. The serum was separated by centrifugation and stored at -80ºC. After the liver tissue was removed, the number of nodules was recorded in detail. Then, part of the liver tissue was fixed in 4% paraformaldehyde solution; the other part was stored at low temperature.

Histopathological examination

Hematoxylin and eosin staining and Masson staining

H&E staining was carried out in accordance with the standard procedure (Feldman and Wolfe., 2014): Briefly, tissue samples (3–5 mm) fixed in 4% formalin were dehydrated, cleared in xylene, and embedded in paraffin. 4 μm sections were then cut onto glass slides, dried, dewaxed with xylene and washed out of the xylene. Stained with hematoxylin for 5 minutes and then counterstained with hydrochloric acid and ammonia solution. Dehydrated with 70% and 90% alcohol, stained with eosin for 3 minutes, dehydrated with 80% and 95% alcohol and soaked in anhydrous ethanol for 15 minutes. After soaking in xylene for 20 minutes, the sections were mounted with a drop of gum. Pathological structural changes in liver tissue were carefully observed under a light microscope. Masson trichrome staining was performed (Zhang *et al*., 2000): The procedure was performed according to kit instructions. Dewaxed and hydrated tissue sections were stained with Ponceau fuchsin, phosphomolybdic acid and aniline blue solutions. After completion, the sections were dehydrated, cleared and mounted. Mounted sections were observed under a light microscope. Collagen fibers appeared blue, myofibers and cytoplasm appeared red and nuclei were blue-black. For each sample group, ≥5 fields of view were randomly selected and analyzed using Image-Pro Plus software to determine the percentage of collagen area within the field of view.

Immunohistochemistry (IHC)

IHC staining used the SP method. Paraffin sections were dewaxed and hydrated, then incubated in 3% H2O2 for 10 minutes, followed by antigen retrieval. Nonspecific antigens were then blocked with 5% BSA. A diluted primary antibody (rabbit anti-Ki-67 polyclonal antibody) was added for overnight incubation at 4ºC. After rinsing with PBS, the secondary antibody solution was added for 30 minutes. The sections were then developed using DAB and counterstained with hematoxylin before mounting. Yellow-brown granular deposits were considered positive under light microscopy.

Serological testing

AFP and IL-1β levels in serum samples were analyzed using ELISA. The specific procedures were performed strictly according to the kit instructions. The absorbance of was measured and the concentrations of AFP and IL-1β in the samples were calculated.

Reactive oxygen species level detection

Tissue homogenate and cell sample preparation: Weigh 20 mg of liver tissue sample and add pre-chilled PBS to the sample, place it in an ice bath and grind it using a homogenizer to prepare a 10% tissue homogenate. The homogenate was centrifuged at 3000 rpm for 10 min at 4ºC. The supernatant was then aspirated. Cells in each group were washed and resuspended at a density of 1×10^6 cells/mL.

DCFH-DA probe loading: DCFH-DA probe (final concentration 10 μM) was added in the dark for 30 minutes. Mix thoroughly every 5 minutes to ensure adequate contact between the probe and the sample.

Detection: After incubation, wash cells to remove the probe molecules. Transfer the prepared cell suspension to a black 96-well plate and add the tissue homogenate sample to a regular 96-well plate. Detect fluorescence intensity using a fluorescence microplate reader.

Western blot analysis

Western blot analysis was performed according to standard procedures (Pillai-Kastoori *et al*., 2020). Briefly, the steps were as follows: *Protein Extraction and Quantification:* Lyse the liver tissue or SMMC-7721 hepatocellular carcinoma cells to be processed on ice for 30 minutes using RIPA lysis buffer. Incubate at 12,000 rpm for 15 minutes, collect the supernatant and analyze using the BCA assay.

Electrophoresis and transfer: Mix 20-40 μg of protein sample with 5× loading buffer, heat-denature and then apply to a 10-12% SDS-PAGE gel for electrophoresis and transfer to the appropriate membrane. Immunoreactivity: PVDF membrane was blocked for 1 h and incubated with primary antibodies against NLRP3 (ab263899, 1:1000), ASC (ab283684, 1:1000), Caspase-1 (ab207802, 1:1000), IL-1β (ab197447, 1:1000), α-SMA (ab240678, 1:1000), GAPDH/β-actin internal control and then with secondary antibodies (1:5000) for 1 h followed by washing and exposure. Protein band images were acquired and saved and the grayscale values of the protein bands were measured.

qRT-PCR assay

Following total RNA extraction using the Trizol method, gene expression levels were detected via quantitative real-time PCR (qRT-PCR) according to the experimental procedures described in prior literature (Jozefczuk and Adjaye, 2011). RNA purity and concentration were measured using a UV spectrophotometer. RNA was reversely transcribed to generate cDNA using miR-145 primers. In the qPCR experiment, the reverse transcribed cDNA served as a template for target gene amplification using SYBR Green qPCR Master Mix.

The total reaction volume was 20 μL. The reaction procedure was as follows: 94ºC 1 min, followed by a temperature drop to 55ºC 1 min, then a temperature increase to 72ºC 1.5 min. This reaction was repeated for 30 cycles with a 5-min extension at 72ºC. mRNA expression was calculated using 2-ΔΔCt method (Table 1).

Cell experiments

Cell culture and grouping

Cell culture and grouping: Human hepatocellular carcinoma cell lines HepG2 and SMMC-7721 were selected because they are widely used in liver fibrosis and HCC research and respond to TGF-β 1-induced activation, making them suitable for modeling key events in liver disease progression. The cells were seeded in high-glucose DMEM medium and transferred to a constant temperature incubator (37ºC, CO_2). When the cells reached the logarithmic growth phase, they were divided into the following groups: Control group: continued culture with standard complete medium; TGF-β1 group: added 10 ng/mL TGF-β1; TGF-β1 + icariin group: in addition to TGF-β1 stimulation, cells were co-treated with different concentrations of icariin (20, 40, 80 μM) for 24 or 48 hours; TGF-β1 + NAC (ROS inhibitor); and TGF-β1 + ICA + 2-ME (ROS activator). Following ICA treatment, cells were co-transfected with miR-145 mimics for functional restoration experiments.

Cell activities assays

Cell Proliferation: SMMC-7721 cells were seeded evenly in a 96-well plate at 5×10^3/well. After cells adhered to the plate, they were grouped. CCK-8 solution (10 μL) was added for 2 hours to measure OD value of each well at 450 nm.

Apoptosis: After digestion, cells in each experimental group were resuspended at 1×10^6/mL. The cells were washed, resuspended and incubated with Annexin V-FITC and PI to measure apoptosis.

Cell migration and invasion assays were performed as previously described with minor modifications (Pijuan *et al*., 2023). *Migration assay*: 200 μL of a serum-free cell suspension at a density of 5×10^4 was added to upper chamber and 600 μL of complete culture medium was added to lower chamber. After 24 hours, cells on inner side of upper chamber membrane that had not migrated were gently wiped away with a clean cotton swab and cells that had successfully migrated to the outer side of the membrane were fixed. Cells were stained with 0.1% crystal violet. Cell counts were performed in five randomly selected fields and absorbance was measured at 565 nm.

Table 1: qRT-PCR primers and primer sequences.

Primers		Sequences (5'-3')
NLRP3	Forward	TGTTGTCAGGATCTCGCATTG
	Reverse	GAGCAGCACAGTGAAGTAAGG
miR-145	Forward	CCTCCGGTCCAGTTTTCCC
	Reverse	CCATGACCTCAAGAACAGTATTTCC
U6	Forward	CTCGCTTCGGCAGCACA
	Reverse	AACGCTTCACGAATTTGCGT

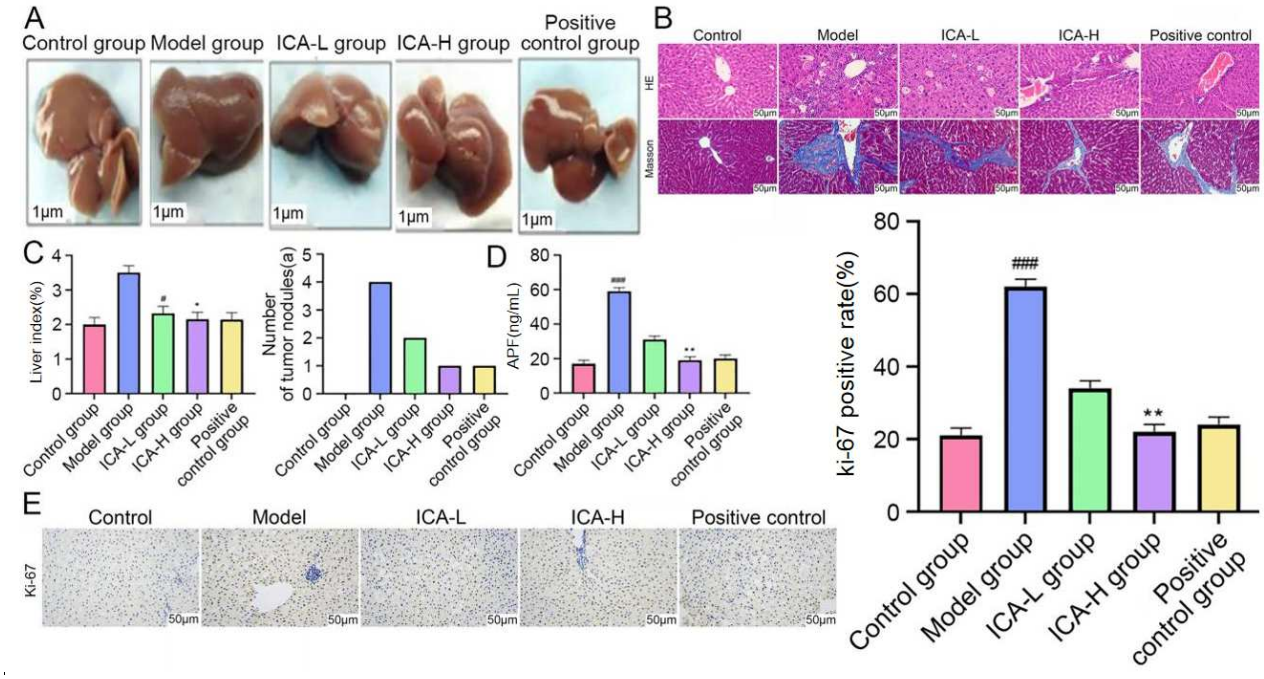

Fig. 1: Icariin alleviates DEN/CCl4-induced liver fibrosis and hepatocarcinogenesis in rats.
Notes: (A) Representative gross photographs of livers; (B) Representative images of H&E and Masson staining of liver tissue; (C) Statistical bar graph of liver index and number of tumor nodules; (D) Statistical graph of serum AFP levels; E: Representative images of Ki-67 immunohistochemistry in liver tissue;

Cell invasion assay: 50 μL of Matrigel was evenly spread on the polycarbonate membrane surface of the upper chamber of the Transwell. After pre-curing, subsequent procedures were performed according to the cell migration assay.

Mechanism verification experiments

To verify the targeting relationship between miR-145 and NLRP3, we performed a dual-luciferase reporter gene assay following standard procedures (Zhang and Zheng, 2025). Reporter plasmids containing wild-type (WT) and mutant (MUT) sequences of NLRP3 gene 3'UTR were constructed and co-transfected with miR-145 mimic into SMMC-7721 and HepG2 cells. After 48 hours, intracellular luciferase activity was measured.

Extracellular miR-145 detection: Exosomes were isolated from cell culture supernatants using differential ultracentrifugation (Theel and Schwaminger, 2022). Total RNA was extracted to analyze miR-145 levels.

Statistical methods

Data were analyzed using SPSS 27.0 and GraphPad Prism 8.02. All datasets were tested for normality using the Shapiro-Wilk test and for homogeneity of variances using Levene's test. Comparisons between two groups were performed using independent samples t-test, while one-way ANOVA was employed for multiple group comparisons. When ANOVA indicated significant differences, post-hoc pairwise comparisons were conducted using the LSD method; in cases of unequal variances, Tamhane's T2 test was applied. The significance level was set at $P < 0.05$, with $P < 0.01$ indicating statistically significant differences.

RESULTS

Icariin alleviates DEN/CCl_4-induced liver fibrosis and hepatocarcinogenesis in rats

A DEN/CCl_4-induced rat hepatocarcinogenesis model was established. As shown in Fig. 1A, livers of rats in model group rats were significantly enlarged, with a rough surface

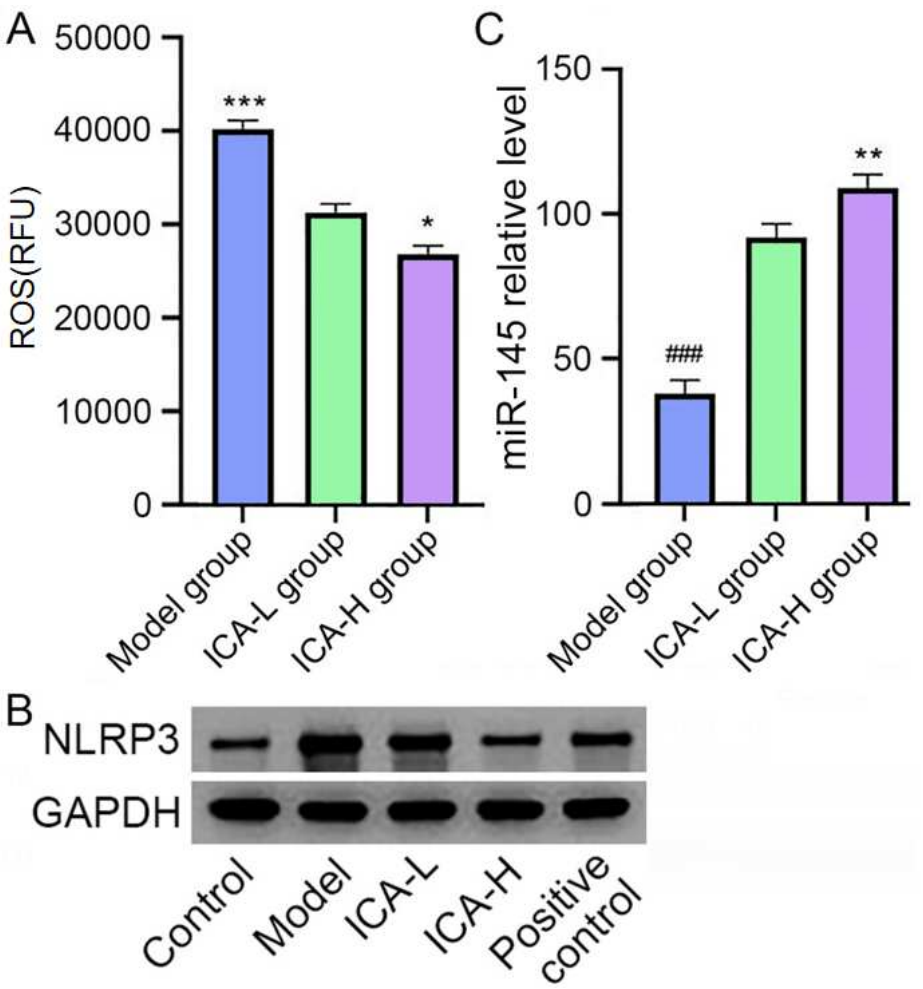

Fig. 2: Icariin inhibits the ROS-NLRP3 inflammasome axis in liver tissue and upregulates miR-145.
Note: (A) ROS levels in liver tissue; (B) Western blot analysis of NLRP3 inflammasome-related proteins; (C) miR-145 expression in liver tissue. *P<0.05, **P<0.01

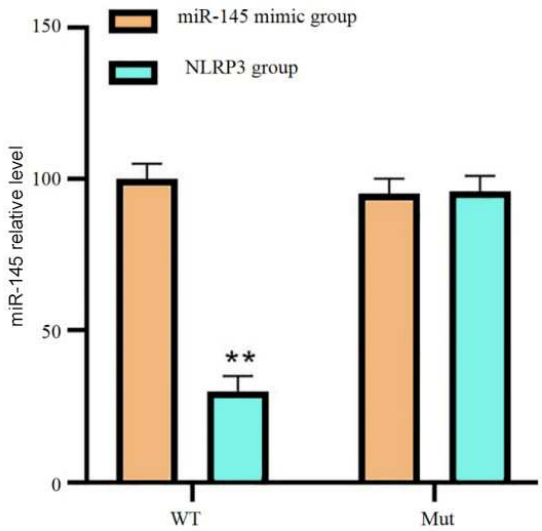

Fig. 3: miR-145 directly inhibits NLRP3 expression.
Note: **P<0.01

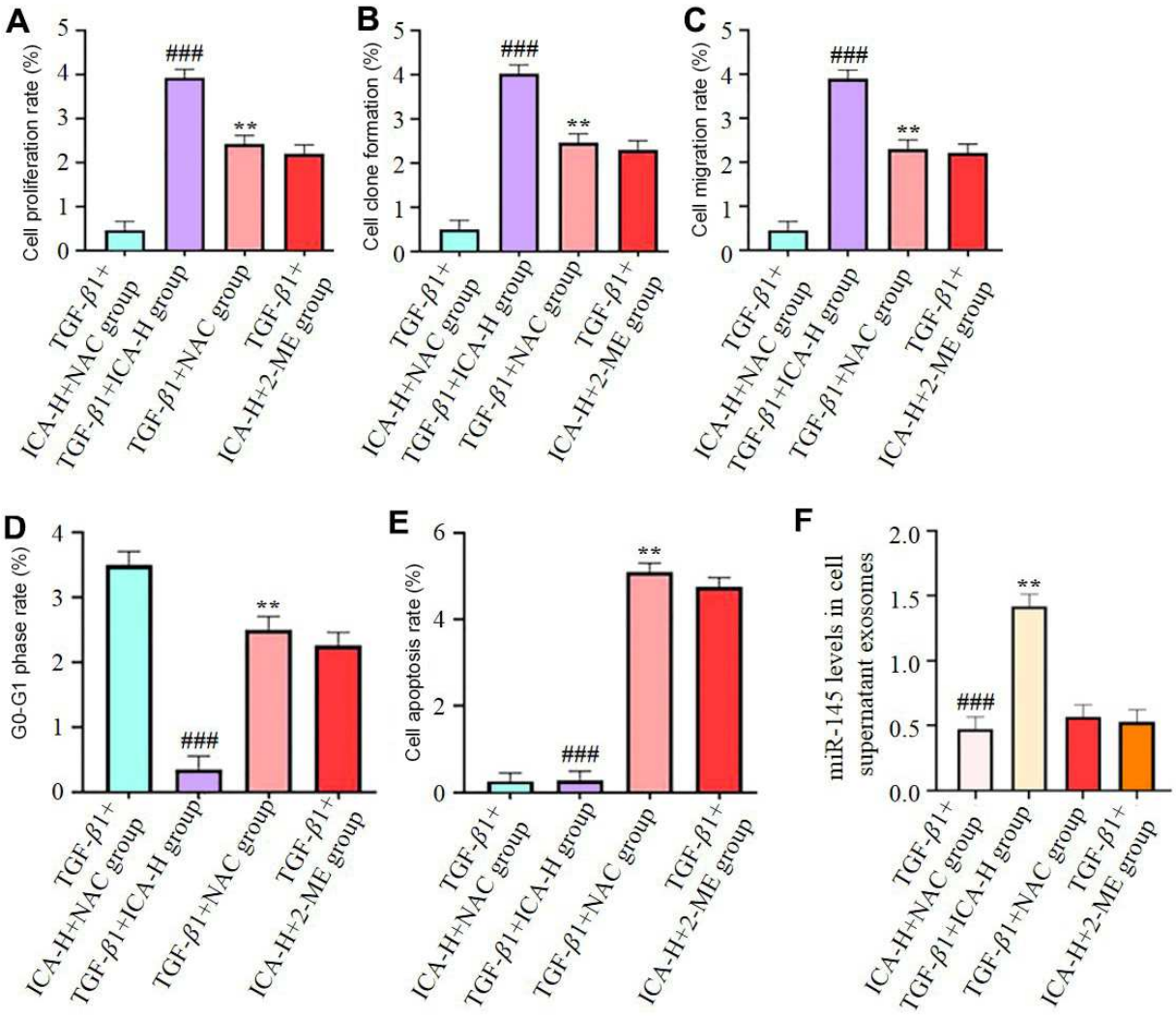

Fig. 4: Icariin inhibits the malignant phenotype of liver cancer SMMC-7721 cells *in-vitro* via the ROS-NLRP3/miR-145 axis. Note: ICA inhibits the (A) proliferation, (B) colony formation, (C) migration, (D) induces G0/G1 arrest, (E) apoptosis of liver cancer SMMC-7721 cells and (F) miR-145 levels in cell supernatant exosomes. *P<0.05, **P<0.01.

and numerous grayish-white tumor nodules. After icariin treatment, the number of surface nodules in the ICA-H group was significantly reduced, and liver texture improved. H&E staining (Fig. 1B) revealed that the normal liver architecture in model group was disrupted, with prominent dysplastic nodules and early cancerous foci, accompanied by pathological mitotic figures. Masson staining (Fig. 1B) revealed that in the model group, abnormal deposition of abundant blue-stained collagen fibers was observed, forming extensive fibrous septa and a typical pseudolobular structure. In addition, the liver index (liver-to-body ratio) was increased in model group (P<0.01), while ICA treatment dose-dependently reduced the liver index. Furthermore, statistical analysis of gross liver specimens revealed a significant increase in the mean number of tumor nodules in model group, while ICA treatment significantly reduced the number and size of nodules (Fig. 1C).

Serum AFP levels were dramatically elevated in the model group, while icariin treatment significantly reduced them (P<0.01; Fig. 1D). Ki-67 immunohistochemistry (Fig. 1E) showed a significant increase in Ki-67-positive cells in the model group, which was reduced by icariin treatment. These proliferating cells were primarily located in dysplastic nodules and cancerous foci.

Icariin inhibits the ROS-NLRP3 inflammasome axis in liver tissue and upregulates miR-145

Fig. 2A shows that ROS levels in liver tissue in Model group were elevated (P<0.01) and reduced after ICA treatment (P < 0.05 or P < 0.01). Western blot analysis (Fig. 2B) showed upregulated NLRP3 expression in model group liver tissue, which was significantly suppressed by icariin intervention. qRT-PCR analysis (Fig. 2C) showed that miR-145 was down regulated in liver tissue from model group rats.

miR-145 directly inhibits NLRP3 expression

miR-145 mimic transfection significantly elevated intracellular miR-145 levels and effectively down regulated NLRP3 mRNA and protein expression (Fig. 3). Furthermore, the effects of miR-145 overexpression were consistent with those of icariin treatment, suggesting that miR-145 is a key downstream effector molecule of ICA.

Icariin inhibits the malignant phenotype of SMMC-7721 liver cancer cells In vitro via the ROS-NLRP3/miR-145 axis

TGF-β1-treated cells were subjected to ROS activation or inhibition. As shown in Fig. 4, ICA treatment significantly inhibited TGF-β1-induced proliferation (Fig. 4A), colony formation (Fig. 4B), migration (Fig. 4C), leading to G0/G1 arrest (Fig. 4D) and a significant increase in the apoptotic rate (Fig. 4E) ($P<0.05$ or $P<0.01$). As shown in Fig. 4F, ICA treatment significantly increased miR-145 levels in exosomes from the supernatant of SMMC-7721 liver cancer cells ($P<0.01$). Treatment with the ROS inhibitor NAC completely blocked ICA-induced upregulation of exosome miR-145.

DISCUSSION

The main pathological features of cirrhosis include diffuse hepatocyte degeneration and necrosis. Further deterioration will lead to fibrosis and nodular regeneration of hepatocytes. In addition, up to 80% of liver cancer patients have underlying diseases such as cirrhosis (Guo *et al*., 2022). Modern medicine currently has no better drugs for anti-liver fibrosis. However, traditional Chinese medicine, with its long history, has shown unique advantages and potential in liver cancer treatment (Shao *et al*., 2024). Using a DEN/CCl_4-induced cirrhosis-carcinogenesis model, we demonstrated that icariin inhibits ROS generation, blocks NLRP3 activation, upregulates miR-145, and thereby attenuates malignant progression in cirrhosis. This study elucidates the molecular mechanism by which icariin inhibits cirrhosis-associated carcinogenesis and suggests its potential clinical application.

Previous studies indicate that icariin inhibits prostate cancer bone metastasis and destruction, suggesting its broad anticancer potential (Chen *et al*., 2023). Flavonoids, alkaloids, etc. are all active ingredients of epimedium, among which epimedium isoprenoid brass and icariin have good anti-liver cancer activity. It has been reported (Ding *et al*., 2023) that icariin possesses immunoenhancing and anti-hepatoma activities. We showed that the liver of model group rats was significantly enlarged, with a rough surface and covered with gray-white tumor nodules and the liver index was significantly increased. The normal structure was destroyed, with obvious dysplastic nodules and pathological nuclear division images. There were multiple blue collagen fibers deposited, forming extensive fibrous septa and pseudolobular structures. At the same time, the serum AFP concentration increased sharply and the Ki-67 positive cell rate in liver tissue was significantly increased. The study (Li *et al*., 2023) showed that the α-fetoprotein level in the Ki-67 high expression group was higher, the diameter of the hepatocellular tumor was larger and the tumor shape was more irregular. Similarly, Hong et al. (2023) found that an elevated liver index correlates with poor prognosis.

After ICA intervention, the number of liver surface nodules was significantly reduced, the texture was improved, ICA treatment could dose-dependently reduce the liver index, the degree of liver tissue damage and nodule formation were significantly reduced, collagen fiber deposition was significantly reduced, AFP levels were significantly reduced and Ki-67 positive cells number was reduced, indicating that icariin can effectively reduce DEN/CCl4-induced liver fibrosis and liver cancer and inhibit liver cells proliferation. Consistently, Gao *et al.* (2025) reported that icariin induces autophagy and apoptosis in HCC cells via the lncRNA LOXL1-AS1/β-catenin axis, supporting our findings.

Inflammation is a process responding to the stimulation of dying cells, irritants or pathogens (Pena *et al*., 2024). Previously, it was found that JDHY inhibited inflammatory factors through the ROS-NLRP3 signaling pathway to alleviate D-Ga1N/LPS-induced liver failure (Li *et al*., 2024), which is similar to the conclusion of this study. Our results showed that ROS levels were significantly increased, NLRP3 was upregulated, and miR-145 was down regulated in model group liver tissue, all of which were reversed by icariin intervention. Chu *et al.* (2023) demonstrated that increased miR-145 levels inhibit tumor metastasis. In addition, miR-145 level in liver tissue was negatively correlated with NLRP3 expression, indicating that icariin can effectively reduce oxidative stress in liver tissue, inhibit the excessive activation of NLRP3 inflammasome and meanwhile upregulate miR-145, which has a potential anti-cancer effect. NLRP3 inflammasome activation is a key contributor to hepatotoxicity (Liu *et al.,* 2025). Thus, inhibiting NLRP3 activation may reduce hepatotoxicity, further supporting our conclusions.

Further dual luciferase reporter gene experiments were performed to verify the relation of miR-145 mimic with NLRP3 (Longo *et al*., 2020) or HepG2 cells (Stanley *et al*., 2022). The results showed that transfection of miR-145 mimic significantly upregulated miR-145 and effectively downregulated NLRP3. The effect of overexpression of miR-145 was consistent with that of icariin treatment, suggesting that miR-145 is a key effector molecule downstream of icariin. To our knowledge, this is the first study to demonstrate that icariin suppresses hepatocarcinogenesis by upregulating miR-145. This finding is extremely important for exploring new targets for treating liver cancer. It has been reported (Chen *et al*.,

2024) that by regulating intracellular ROS levels and NLRP3, Caspase family proteins can be activated to induce cell pyroptosis—a process that may exacerbate hepatocyte damage, further confirming the importance of ROS-NLRP3 signaling in mediating hepatocyte inflammation and death. In addition, this study aimed to verify *in vitro* whether icariin acts through the ROS-NLRP3/miR-145 axis, using TGF-β1 stimulation in SMMC-7721 and HepG2 cell models for validation. Icariin treatment significantly inhibited TGF-β1-induced proliferation, colony formation, migration and invasion of SMMC-7721 liver cancer cells. This suggests that icariin can effectively reverse the activation and malignant phenotype of SMMC-7721 liver cancer cells and ameliorate the malignant progression of hepatocellular carcinoma in patients with cirrhosis. However, this study has limitations, as it did not fully explore downstream factors of miR-145. Future research is warranted to further assess the role of icariin in treating liver cancer.

CONCLUSION

In summary, icariin can inhibit ROS-NLRP3 signaling, thereby upregulating miR-145 and inhibiting the malignant transformation of cirrhotic patients. This provides theoretical support for the development of preventive strategies and clinical treatment of cirrhosis and liver cancer.

Acknowledgment
Joint Guidance Project of Qiqihar Science and Technology Plan (LSFGG-2025102)

Authors' contributions
Xiangda Meng and Shimin Wang: Research design, experimental operations, data collection and analysis, manuscript writing and revision; Jing Zhang, Hongting Sui and Guohua Li: Experimental implementation, data organization, statistical analysis and chart preparation; Liping Cong and Wenjuan Wang: Cell experiments, molecular mechanism validation and literature research; Chao Wu and Ting Cao: Animal model establishment, pathological analysis and manuscript review; Yanfei Wang: Project guidance, research supervision, funding support and final manuscript approval.

Funding
There was no funding.

Data availability statement
The datasets generated and/or analyzed during the current study are available from the corresponding author upon reasonable request.

Ethical approval
This study was approved by the ethics committee of Qiqihar Medical University First Affiliated Hospital (Lunshen) 2025 (Research) No. 012-001.

Conflict of interest
The authors declare that the research was conducted in the absence of any commercial or financial relationships that could be construed as a potential conflict of interest.

REFERENCES

Carpi S, Daniele S, De Almeida J F M and Gabbia D (2024). Recent advances in miRNA-Based therapy for MASLD/MASH and MASH-associated HCC. *Int J Mol Sci.,* **25**(22): 12229.

Chen C, Wang S, Wang N, Zheng Y, Zhou J, Hong M, Chen Z, Wang S, Wang Z and Xiang S (2023). Icariin inhibits prostate cancer bone metastasis and destruction via suppressing TAM/CCL5-mediated osteoclastogenesis. *Phytomedicine.,* **120**: 155076.

Chen W, Yang K B, Zhang Y Z, Lin Z S, Chen J W, Qi S F, Wu C F, Feng G K, Yang D J, Chen M, Zhu X F and Li X (2024). Synthetic lethality of combined ULK1 defection and p53 restoration induce pyroptosis by directly upregulating GSDME transcription and cleavage activation through ROS/NLRP3 signaling. *J Exp Clin Cancer Res*., **43**(1): 248.

Chu D X, Jin Y, Wang B R, Jiao Y, Zhang C K, Guo Z H, Hu SZ and Li N (2023). LncRNA HOTAIR enhances epithelial-to-mesenchymal transition to promote the migration and invasion of liver cancer by regulating NUAK1 via epigenetic inhibition miR-145-5p Expression. *J Cancer.,* **14**(12): 2329–2343.

Ding Y, Yu B, Zhou S, Ding C, Zhang Z, Xu S and Xu Z (2023). Improvement of solubility and pharmacokinetic profile of hepatoprotector icariin through complexation with HP-γ-cyclodextrin. *Front Pharmacol.,* **14**: 1138686.

Feldman AT and Wolfe D (2014). Tissue processing and hematoxylin and eosin staining. *Methods Mol Biol*., **1180**: 31–43.

Gao S, Zhang W, Dai J, Hu W, Xu Y, Yang H, Ye B, Ouyang H, Tang Q, Zhao G and Zhu J (2025). Icariin mediates autophagy and apoptosis of hepatocellular carcinoma cells induced by the β-catenin signaling pathway through lncRNA LOXL1-AS1. *Naunyn Schmiedebergs Arch Pharmacol.,* **398**(7): 8455–8468.

Guo W, Ge X, Lu J, Xu X, Gao J, Wang Q, Song C, Zhang Q and Yu C (2022). Diet and risk of non-alcoholic fatty liver disease, cirrhosis and liver cancer: A large prospective cohort study in UK Biobank. *Nutrients.,* **14**(24): 5335.

Hai Y, Zuo L, Wang M, Zhang R, Wang M, Ren L, Yang C and Wang J (2023). Icariin alleviates nonalcoholic fatty liver disease in polycystic ovary syndrome by improving liver fatty acid oxidation and inhibiting lipid accumulation. *Molecules.,* **28**(2): 517.

Hong C, Dong HZ, Li RN, Zhu HB, Li QM, Cui H, Hu CY, Huang CY, Peng J, Liu L, Zou XJ and Xiao LS (2023). Predictive value of the hepatic immune predictive index for patients with primary liver cancer treated with immune checkpoint inhibitors. *Dig Dis.,* **41**(3): 422–430.

Hwang SY, Danpanichkul P, Agopian V, Mehta N, Parikh ND, Abou-Alfa GK, Singal AG and Yang JD (2025). Hepatocellular carcinoma: Updates on epidemiology, surveillance, diagnosis and treatment. *Clin Mol Hepatol.,* **31**(Suppl): S228–S254.

Jozefczuk J and Adjaye J (2011). Quantitative real-time PCR-based analysis of gene expression. *Methods Enzymol*., **500**: 99-109.

Lai Y, Liu J, Hu X, Zeng X and Gao P (2023). Modifications of the human liver cancer cells through microRNA-145-mediated targeting of CDCA3. *Cell J.,* **25**(8): 546–553.

Li C Y, Lin Y, Ding X, Zhang P, Liao L Z and Yue X (2023). *Zhonghua Yi Xue Za Zhi.,* **103**(47): 3835–3841.

Li F, Guan Z, Gao Y, Bai Y, Zhan X, Ji X, Xu J, Zhou H and Rao Z (2024). ER stress promotes mitochondrial calcium overload and activates the ROS/NLRP3 axis to mediate fatty liver ischemic injury. *Hepatol Commun.,* **8**(4): e0399.

Liu Y, Liu B, Shi M, Ye T and Li H (2025). NLRP3 Inflammasome activation is involved in geniposide-induced hepatotoxicity. *Mediators Inflamm.,* **2025***:* 4112856.

Longo L, Tonin Ferrari J, Rampelotto P H, Hirata Dellavia G, Pasqualotto A, P Oliveira C, Thadeu Schmidt Cerski C, Reverbel da Silveira T, Uribe-Cruz C and Álvares-da-Silva M R (2020). Gut dysbiosis and increased intestinal permeability drive microRNAs, NLRP-3 inflammasome and liver fibrosis in a nutritional model of non-alcoholic steatohepatitis in adult male sprague dawley rats. *Clin Exp Gastroenterol*., **13***:* 351–368.

Peña O A and Martin P (2024). Cellular and molecular mechanisms of skin wound healing. *Nat Rev Mol Cell Biol.,* **25**(8): 599–616.

Pijuan J, Macia A and Panosa A (2023). Live cell adhesion, migration, and invasion assays. *Methods Mol Biol*., **2644**: 313-329.

Pillai-Kastoori L, Schutz-Geschwender AR and Harford JA (2020). A systematic approach to quantitative Western blot analysis. *Anal Biochem*., **593**: 113608.

Rong J, Liu T, Yin X, Shao M, Zhu K, Li B, Wang S, Zhu Y, Zhang S, Yin L, Liu Q, Wang X and Zhang L (2024). Co-delivery of camptothecin and MiR-145 by lipid nanoparticles for MRI-visible targeted therapy of hepatocellular carcinoma. *J Exp Clin Cancer Res.,* **43**(1): 247.

Shao G, Liu Y, Lu L, Wang L, Ji G and Xu H (2024). Therapeutic potential of traditional Chinese medicine in the prevention and treatment of digestive inflammatory cancer transformation: *Portulaca oleracea* L. as a promising drug. *J Ethnopharmacol.,* **327***:* 117999.

Shen J, Wang Z, Liu M, Zhu YJ, Zheng L, Wang LL, Cheng JL, Liu TT, Zhang GD, Yang TY, Wang X and Zhang L (2023). LincRNA-ROR/miR-145/ZEB2 regulates liver fibrosis by modulating HERC5-mediated p53 ISGylation. *FASEB J.,* **37**(6): e22936.

Singal A G, Kanwal F and Llovet J M (2023). Global trends in hepatocellular carcinoma epidemiology: Implications for screening, prevention and therapy. *Nat Rev Clin Oncol.,* **20**(12): 864–884.

Stanley L A and Wolf C R (2022). Through a glass, darkly? HepaRG and HepG2 cells as models of human phase I drug metabolism. *Drug Metab Rev*., **54**(1): 46–62.

Theel EK and Schwaminger SP (2022). Microfluidic approaches for affinity-based exosome separation. *Int J Mol Sci*., **23**(16): 9004.

Uehara T, Pogribny IP and Rusyn I (2021). The DEN and CCl4-induced mouse model of fibrosis and inflammation-associated hepatocellular carcinoma. *Curr Protoc.,* **1**(8): e211.

Wang K, Liu H, Sun W, Guo J, Jiang Z, Xu S snd Miao Z (2023). Eucalyptol alleviates avermectin exposure-induced apoptosis and necroptosis of grass carp hepatocytes by regulating ROS/NLRP3 axis. *Aquat Toxicol.,* **264***:* 106739.

Zhai L, Pei H, Yang Y, Zhu Y and Ruan S (2022). NOX4 promotes Kupffer cell inflammatory response via ROS-NLRP3 to aggravate liver inflammatory injury in acute liver injury. *Aging.,* **14**(17): 6905–6916.

Zhang J, You H, Wang T, Wang B, Jia J, Katayama H, Maeda S, Wang R, Asano G, Ishiwata T, Naito Z and Yokoyama M (2000). Triple-staining to identify apoptosis of hepatic cells in situ. *J Nippon Med Sch*.i, **67**(4): 280–283.

Zhang R and Zheng H (2025). Luciferase reporter assay for determining the signaling activity of interferons. *Methods Mol Biol*., **2854**: 19-28.